COBEM 2021 26th International Congress of Mechanical Engineering
November 22-26, 2021, Virtual Congress, Brazil
ABCM Associação Brasileira de Engenharia e Ciências Mecânicas

# COB-2021-0468
# OPTIMAL PRELIMINARY SIZING AND ANALYSIS OF ELECTROMECHANICAL ACTUATOR WITH BOND GRAPH

**Caio Bromonschenkel Paes**
**Luiz Carlos Sandoval Góes**
Instituto Tecnológico de Aeronáutica - ITA, CTA - Praça Marechal do Ar Eduardo Gomes 50 - São José dos Campos - SP - 12228-900 - Brazil
caiopaes@ita.br
goes@ita.br

**Raphael das Neves Calvo**
Empresa Brasileira de Aeronáutica - EMBRAER, Av. Brigadeiro Faria Lima 2170 - São José dos Campos - SP - 12227-901 - Brazil
raphael.calvo@embraer.com.br

***Abstract.*** *The aeronautics industry has always been looking for innovations capable of providing reductions in operational costs and, more recently, it started the search for greener solutions. The major contributor to the operational costs and emissions is the consumption of aviation fuel. However, maintenance activities also play an important role in the composition of operational expenses. Therefore, solutions capable of providing a higher overall energetic efficiency while requiring less maintenance are of utmost importance for aircraft manufacturers. In this context, efforts to substitute conventional hydro-mechanical systems for electric systems are becoming increasingly common, originating the concept of more-electric aircraft. In the field of flight control, electromechanical actuators have been studied as a solution to replace conventional actuators. This work's goal is to provide the means to allow viability studies regarding this trade-off from a power demand and actuator weight perspective. In order to do so, the development of two different tools that should aid the decision making process in the electromechanical actuator viability studies is proposed. The first tool consists on an actuator preliminary sizing tool which allows both demanded power and actuator mass estimation based on the project requirements. The second tool consists on a simulation environment for the actuator based on a mathematical model obtained by using the bond graph method. Both tools are described and a case study is presented to explore their capabilities and to show how their use can be helpful in a preliminary sizing context.*

***Keywords:*** *Electromechanical Actuator, Bond Graph, Optimization, Modeling*

## 1. INTRODUCTION

Motivated by the trend to reduce costs associated to fuel consumption and the need for greener aircraft, the aerospace industry is currently taking steps towards increasing the use of electrically powered equipment. In such context, efforts to replace conventional hydraulic, pneumatic and mechanically powered systems with electrically powered systems have arisen. Such aircraft concept is usually referred as the *more-electric aircraft*.

Electro-hydrostatic actuators (EHA) and electromechanical actuators (EMA) present themselves as solutions for the electrification of flight control systems, replacing the conventional actuation technology, which makes use of servo actuators fed by a central hydraulic power distribution system. However, even though EHAs are electrically powered, they still rely on a local hydraulic network. EMAs, on the contrary, are independent of hydraulic technology to transmit power, and so are capable of providing further benefits in terms of maintainability. Despite these advantages, the maturity of EMAs for commercial aircraft flight control applications is still low due to considerations associated with its power density and response to failure characteristics, as already observed by manufacturers such as Airbus (Todeschi, 2011), whose A380, A400M and A350 aircraft models explore the more-electric concept.

In the works of Budinger *et al.* (2013), the concern regarding the sizing of EMAs for mass and power demand estimation is studied, and a methodology for its optimal preliminary sizing is proposed. However a simplified actuator model is used to validate the sizing results and to allow simulations of its response characteristics when subject to different operation conditions. On the other hand, a detailed approach for virtual prototyping of EMAs is proposed in the works of Fu *et al.* (2018). The different physical effects that must be taken into account when modeling this type of actuator are described and are gradually implemented by using the bond graph formalism.

This work aims to provide the tools to allow a better investigation of the viability of introducing EMAs in a flight control system. A sizing tool inspired by the methodology developed by Budinger *et al.* (2013) is proposed in order to

combine the performance requirements specified for the control surface actuation task and data from EMA components manufacturers catalogs. These informations are inserted in an optimal sizing routine which provides an EMA specification suited for the studied application. Additionally, an EMA model based on the works of Fu *et al.* (2018) is developed to allow the verification of the result from the sizing tool. Such model also allows the preliminary evaluation of the actuator in different conditions of operation while taking complex phenomena such as backlash, pre-load and friction modeling into account. Therefore, these resources shall enable a comparison between the conventional solution and an EMA in the early stages of the flight control system design by addressing the most relevant design concerns. The use of these tools is illustrated by presenting an example of its practical applications.

## 2. ELECTROMECHANICAL ACTUATORS

The EMA studied for flight control applications usually consists of an assembly of components which promote the conversion of electric energy into mechanical energy used to displace a control surface. Such components are each responsible for different tasks required in order to achieve the global function of surface actuation. Energy conversion from the electric to the mechanical domain is performed by an electric motor. However, it may still be desirable to being able to transform the motor's shaft high speed and lower torque into a higher torque at a lower rotation. In this case, a gear train is introduced to adjust the desired output torque and speed. On top of that, the rotary motion provided by the gear train can be converted into a linear displacement by means of a screw mechanism. These components compose the core actuator module of an EMA, which is illustrated in Fig. 1, and, as flight control systems usually employ linear displacement actuators, this architecture is considered as a baseline for this work.

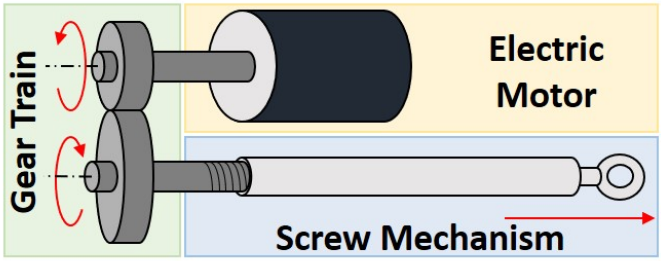


Figure 1: Simplified schematic of EMA core actuator module.

Additional components are required to provide the actuator with an adequate behavior. The capacity of tracking a desired input command is achieved by using power drive electronics (PDE) to modulate the motor power supply. Sensors installed in the EMA provide position, velocity and current information to the PDE, which performs feedback control and current limitation. Also, in order to prevent the actuator from back-driving due to the aerodynamic load applied on the control surface, anti-backdrive mechanisms such as a no-back device attached to the screw mechanism or brakes coupled to the motor shaft are used, providing the motion irreversibility.

As aerospace applications are extremely safety-critical, the aforementioned components are usually combined in an architecture which provides the required levels of availability and integrity for the surface actuation task. Multiple independent motors and/or mechanical paths can be assembled in a single EMA unit. Furthermore, design requirements specify limitations on control surface static and dynamic characteristics (e.g.: surface free-play and stiffness) in order to avoid the occurrence of aeroelastic instabilities. Such specifications are of utmost importance for EMAs, specially regarding free-play, as hydraulic components are replaced by mechanical components subject to wear.

Besides safety requirements, the EMA components are also chosen in order to comply with performance requirements derived from the desired aircraft flight control system behavior. Such requirements are presented as typical control loop requirements (e.g.: settling time, overshoot, maximum rate, gain margin, phase margin, etc.) given expected aerodynamic loads (hinge moments) and reference inputs (pilot commands).

In this work, these design requirements are used to drive an actuator sizing tool which is capable of exploring different combinations of components models and finding the one which is most suited for the application needs. Therefore, the first step to develop the tool is to define the characteristics of the required actuator, narrowing down the available space of solutions. Due to the needs of the application, it is defined that a linear irreversible geared EMA shall result from the sizing routine, and the sizing procedure of each of its components is presented in the following section. Also, redundant elements are not considered for sizing purposes.

## 3. ELECTROMECHANICAL ACTUATOR SIZING TOOL

The developed EMA sizing tool can be divided into two different routines: one dedicated to the evaluation of the sizing equations and another one dedicated to finding an optimal solution. This section starts by presenting further details on the sizing routine and then the optimization problem which must be solved by the tool is described.

### 3.1 Sizing routine

The sizing routine is composed by a module responsible for transforming the actuator performance requirements into components specification. When performing the sizing activity, it is important that the assumptions used to define the components characteristics are such that the final product is representative of a commercial off-the-shelf solution. In order to do so, sizing equations are combined with manufacturers catalogs which are interpolated to allow a reasonable estimation of components properties (e.g.: mass, inertia, load rating, etc.).

As mentioned above, the sizing routine depends on the specification of performance requirements. Therefore, the first step when developing the EMA sizing tool shall be to provide the desired requirements. Such inputs are provided as two major elements: a dynamic response which complies with the desired control loop requirements and a specification of the limiting aerodynamic load which the surface must overcome. By using this data, the sizing routine is executed following the breakdown representation from Fig. 2.

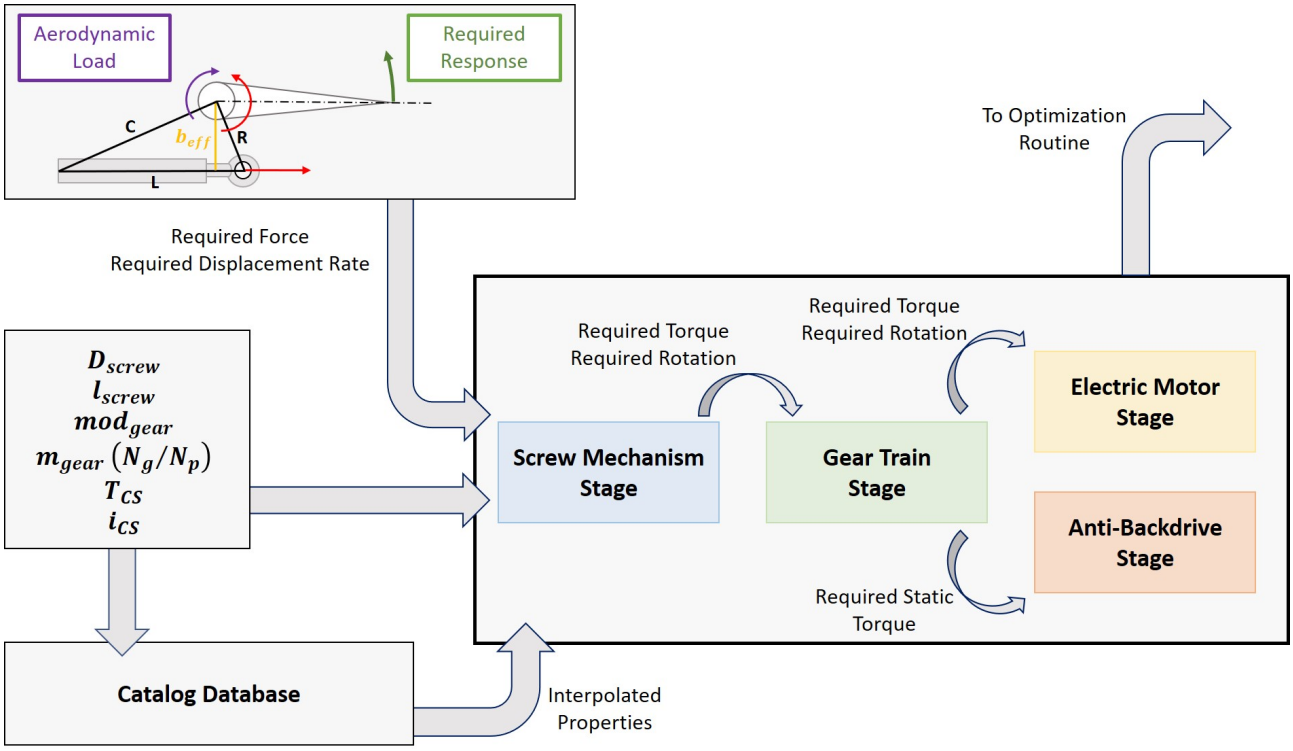


Figure 2: Overview of the sizing routine.

The first stage of the sizing routine takes into account the geometry of control surface installation. Hinge moment and surface deflection are converted to the load acting on the actuator rod and its displacement by using geometrical relations (e.g.: installation effective arm, $b_{eff}$). In order to compute such relations, the installation geometry is assumed to follow an RLC triangle pattern which is displayed in Fig. 2. The values for each size of the RLC triangle, as well as the limits of surface deflection, are defined according to the application needs. With the outputs from this stage, it is possible to proceed to the next stage, where the screw mechanism is sized.

In order to proceed with the sizing of a screw mechanism for the EMA, it is necessary to specify which type of screw mechanism must be evaluated by the routine. Different types of screw mechanism include ACME screws, ball screws and roller screws. Moreover, each one of these alternatives presents different properties which may benefit or not the final actuator design. Due to its high efficiency and adequate load rating or lifetime characteristics, the ball screw is considered as the screw mechanism to be sized. Data to allow estimation of ball screw properties is extracted from THK (2020), and interpolation equations for its mass, inertia, load rating and efficiency are derived from the catalog in terms of the screw diameter ($D_{screw}$) and lead ($l_{screw}$). Then, the performance requirements are transmitted to the gear train module by converting the screw displacement and force into the driven shaft rotation and torque by using the screw ratio ($\frac{l_{screw}}{2\pi}$).

Similar to what was done with the screw mechanism, a particular type of gear train must be selected in order to allow for data extraction from catalogs. In this case, different gear assemblies are viable, and, differently from the screw mechanisms, their benefits are not as easy to evaluate qualitatively. Therefore, the sizing tool is developed to handle different types of gear assemblies: spur, helical, bevel, hypoid and worm gears. By doing so, configurations with different types of reducers can be evaluated and compared against each other to allow a quantitative analysis of the consequences of selecting a particular type. Catalog data from KHK (2015) is used to generate interpolation equations for the gears masses, inertias, torque ratings, efficiency and backlash, in terms of the gear module ($mod_{gear}$) and ratio ($m_{gear}$). Depending on the selected gear type, the gear ratio may have to be defined from the ratio between the driven gear number of teeth ($N_g$) and the driver gear number of teeth ($N_p$). Then, $m_{gear}$ is used to convert the driven shaft torque and rotation into the driver shaft torque and rotation, and this information is forwarded to the anti-backdrive device and electric motor stages.

The anti-backdrive module is a simple stage, but essential to attain the desired actuation irreversibility. By interacting with the gear train module, an anti-backdrive device is selected based on the torque demand. Due to the lack of available no-back data, as an early stage of the sizing tool, it is defined that viable electromagnetic brakes are to be investigated by the routine. Further developments shall include the sizing of a no-back device. Data from OGURA (2012) is used to interpolate the brake mass as a function of the required static torque to maintain the actuation irreversibility.

Selection of an appropriate electric motor type for flight control applications depends on its capacity to provide safe operation while providing a high torque and a compact design. Based on arguments from Cao *et al.* (2012), the brushless dc (BLDC) motor is selected as the motor to be sized for the given application due to its beneficial power-to-weight ratio, efficiency and appropriate fault tolerance. With this in mind, data from PACIFIC SCIENTIFIC (2001) is used to interpolate the motor mass, rotor inertia, torque capacity and voltage constant as functions of the motor continuous stall torque ($T_{CS}$) and current ($i_{CS}$). The required torque obtained from the gear train stage, which is the amount required to withstand the aerodynamic load, is combined with the torque required to provide the acceleration of the overall system, which takes the dynamics of the response into account, to compute the torque that the specified motor must generate. Also, the motor torque constant is defined from the ratio $\frac{T_{CS}}{i_{CS}}$, which is used to evaluate the motor current required to generate such torque.

By the end of the sizing routine, a combination of components defined by $D_{screw}$, $l_{screw}$, $mod_{gear}$, $m_{gear}$ (or $N_p/N_g$), $T_{CS}$, $i_{CS}$, and a possible EMA with a calculated mass and power demand is found. In order to investigate if such solution is in fact capable of providing the required performance and if it can be improved in order to better suit the project needs, this routine is inserted in an optimization routine. The description of the optimization problem that must be solved and how both modules are integrated to compose the EMA sizing tool is presented as follows.

### 3.2 Optimization problem

In order to find an optimal design according to the application needs, an optimization problem is defined. In a summarized manner, an optimization problem consists in finding a set of solutions $x^\star$ which minimizes an objective function $f(x)$ within a given interval . The problem can be such that it is subject to constraints, which can be of linear or non-linear type, and correspond to equalities or inequalities. Thus, the sizing routine can be used to define a problem which fits into these standards.

From the definition of the sizing steps, it is clear that the vector $x$ which must be varied in order to optimize the desired objective is the vector containing the design variables used to interpolate the catalog database, namely $D_{screw}$, $l_{screw}$, $mod_{gear}$, $m_{gear}$ (or $N_p/N_g$), $T_{CS}$, $i_{CS}$. This vector shall then be iterated according to the chosen implemented algorithm in order to minimize the objective function $f(x)$ .

When defining the objective function, one must understand the overall project priorities. Normally, it is desired to find the lightest actuator capable of providing the required performance. By doing so, the overall aircraft weight is reduced, leading to lower fuel consumption and gases emissions. However, it may also be interesting to minimize the peak current demanded by the EMA. Higher currents suggest the need for heavier electric wiring components. Depending on the aircraft size, heavier wiring components may have a larger impact on the overall aircraft weight than simply reducing the actuators weights. As both cited objectives may not be directly related to each other, it may be interesting to allow setting the minimization of both of them. Instead of opting for a multi-objective optimization problem, both the EMA mass $M_{ema}(x)$ and the demanded current $i_{peak}(x)$ can be combined into a single objective by defining an aggregate objective function in which each term is related to a relative importance.

The final step required to define the optimization problem is to describe the constraints which limit the selection of the design variables in $x$. The first set of constraints is related to the load rating of each one of the core components (electric motor, gear train and screw mechanism). As mentioned before, given the values of the variables in $x$, the sizing routine used the interpolations from the catalogs to find the load ratings for each of these components. Another constraint is related to the electrically limiting velocity, which defines if the peak motor rotation obtained from the sizing routine is feasible for the motor specified by $x$. One last constraint is added to guarantee that the specified EMA can attain the specified maximum allowable free-play in order to avoid aeroelastic instabilities.

In summary, the described optimization problem consists in solving Eq. 1 such that Eq. 2 is satisfied. In Eq. 1,

$f(x)$ is the objective function written as an aggregate function in which $\alpha_1$ and $\alpha_2$ are the relative importances of the minimization of $M_{ema}$ and $i_{peak}$, respectively. The solution to this problem must be found within the interval defined by the lower bounds vector ($x_{lb}$) and upper bounds vector ($x_{ub}$), which shall be defined according to the data available in the catalogs. Equation 2 presents the problem constraints, which are represented as inequalities through $C(x)$. $F_{screw}$, $T_{pinion}$, $T_{gear}$ and $T_{motor}$ are the loads on the ball screw, driver gear, driven gear and motor, respectively. The terms with the subscript "rating" are the interpolated load ratings for each one of these components. $\omega_{motor}$ is the motor rotation, $U_S$ is the voltage supplied to the motor and $K_V$ is its voltage constant. These are used to define the electrically limiting velocity constraint. Finally, $b$ is the backlash found from catalog interpolation of the components, and $b_{lim}$ represents the limit value according to the aviation standards.

$$\min_x f(x) = \alpha_1 M_{ema}(x) + \alpha_2 i_{peak}(x), \qquad x_{lb} \leq x \leq x_{ub} \tag{1}$$

$$C(x) = \begin{bmatrix} \max\left[F_{screw}(t,x)\right] - F_{rating,screw}(x) \\ \max\left[T_{pinion}(t,x)\right] - T_{rating,pinion}(x) \\ \max\left[T_{gear}(t,x)\right] - T_{rating,gear}(x) \\ \max\left[T_{motor}(t,x)\right] - T_{rating,motor}(x) \\ \max\left[\omega_{motor}(t,x)\right] - \frac{U_S}{K_V(x)} \\ b(x) - b_{lim} \end{bmatrix} \leq 0 \tag{2}$$

Once the problem is defined according to the above equations, it is possible to use an optimization routine to solve it. As the catalog data is interpolated to generate continuous equations for the components properties, the *Matlab* function *fmincon*, used for finding the minimum of a constrained nonlinear multivariable continuous function, can be used. The optimization tool is then set as illustrated by the schematics in Fig. 3. After defining an initial guess $x_0$ for the design variables, the sizing routine is used to calculate the properties of the specified EMA, and to evaluate both the objective function and constraints by using Eqs. 1 and 2, respectively. The *fmincon* function then uses the interior-point optimization algorithm to generate a new guess for $x$ according to the results from the sizing routine. The new $x$ is fed to the sizing routine and the cycle repeats until the algorithm interprets $x$ as the optimal solution within the specified tolerance.

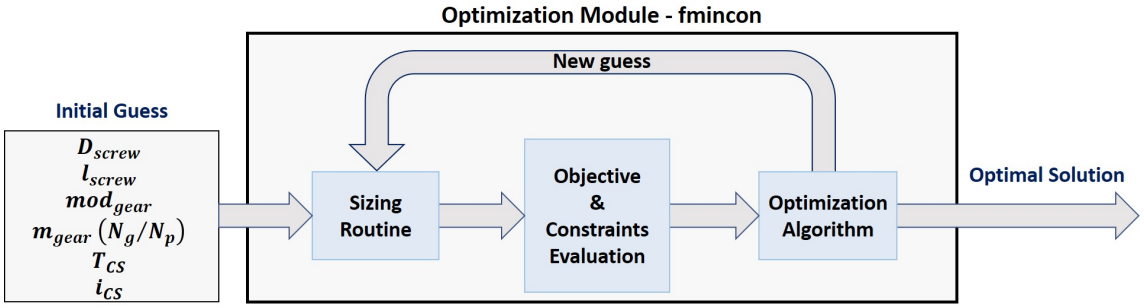


Figure 3: Overview of the optimization routine.

By the end of the optimization routine, a potential optimal combination of components defined by the elements of $x$ is found. However, the continuous variation of $x$ must still be adjusted to fit the models available from the catalogs to define an actual off-the-shelf actuator. Although this moves the sized actuator away from the optimal design, it is essential to allow a feasible product. Also, by using the sizing routine in conjunction with sampling methods, it is possible to evaluate the consequences of varying the design variables in the region near the optimal solution, allowing the prediction of the consequences of such needed approximation.

## 4. ELECTROMECHANICAL ACTUATOR MODEL

After finding the components combination which approximates the optimal solution the most, a final step is required to validate the sized actuator. In order to verify if the solution is really capable of providing the required performance when considering more realistic dynamic phenomena, a model for the EMA is developed and implemented to allow testing through simulations. By doing so, it is possible to verify if the sized actuator actually suits the application, or if adjustments to the design are required until a definitive solution is found.

The bond graph method is used to facilitate the task of performing the multi-domain modeling and definition of governing equations due to its unifying approach. Thus, a bond graph representation of the studied EMA is presented in Fig. 4. Such representation is inspired in the works of Fu *et al.* (2018) on direct gear EMAs. Modifications required to implement the gear train, anti-backdrive mechanism and control surface installation were added to the reference model in order to suit the current study needs. Governing equations are then extracted from the diagram and implemented as a *Simulink* model used to run the simulations.

For the purpose of describing the phenomena included in the proposed model, the bong graph in Fig. 4 is divided into three regions. The region delimited by the yellow lines represents the BLDC motor and its power drive electronics. The region delimited by the green lines represents the gear train and the electromagnetic brakes. Finally, the region delimited by the blue lines represents the ball screw, no-back device and control surface assembly. Note that, despite not included in the sizing routine, the no-back is included in the model as its representation is similar to that of the brakes and its implementation on the tool is predicted on further developments. Also, the gray arrows indicate which terms are responsible for modulating the elements of the bond graph. Description of each included element is presented below according to the proposed diagram subdivision.

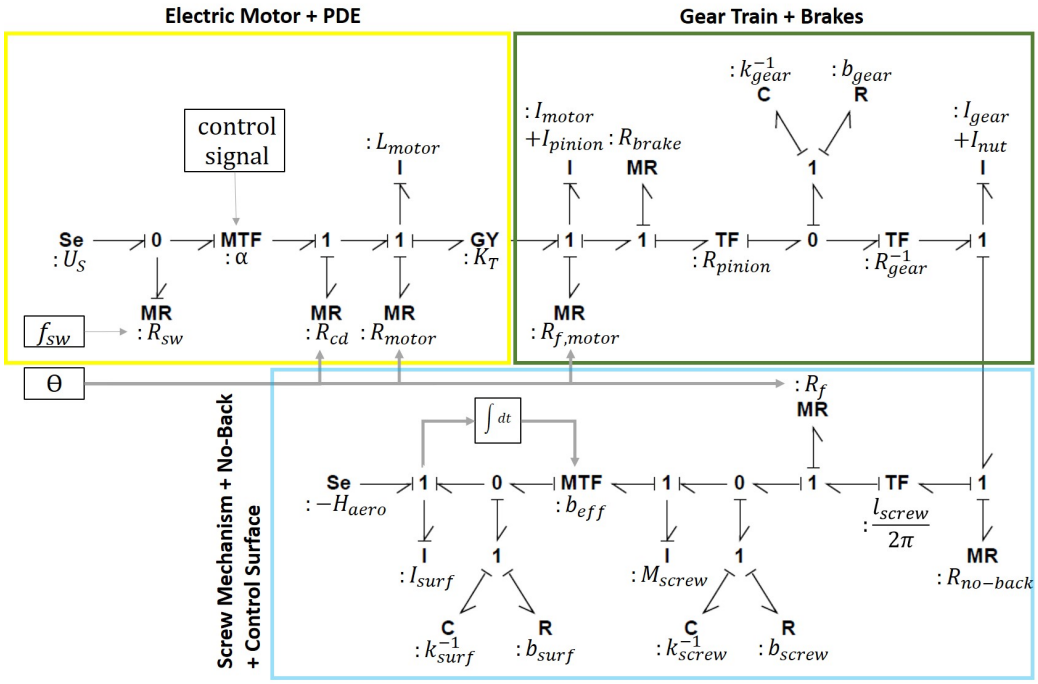

Figure 4: Bond graph representation of the EMA.

### 4.1 Electric motor and power drive electronics

Modeling of the power drive electronics aims to represent a pulse width modulation (PWM) inverter bridge by introducing a perfect transformer element characterized by the ratio $\alpha$, which varies from $-1$ to 1 according to a control signal. Given the voltage supplied by the aircraft electric system $U_S$, the voltage supplied to the motor windings is calculated as $\alpha U_S$. Dissipation effects are included to model switching losses, which depend on the switching frequency $f_{sw}$, and conduction losses, by introducing the R-elements $R_{sw}$ and $R_{cd}$, respectively.

A simplified control scheme is assumed to provide input tracking capability to the modeled EMA. The control of an EMA usually relies on position sensors, such as linear variable differential transformer (LVDT) devices attached to the screw rod, and velocity sensors, such as hall effect sensors installed on the motor. In this work, a cascade structure as represented in Fig. 5 is used. The first stage consists on rod position feedback followed by a proportional gain $K_p$. In this stage, a reference position command is converted to a velocity demand signal. Next, velocity feedback is provided and a new proportional gain $K_v$ is introduced, converting the reference velocity into a torque demand signal. Finally, realization of the power drive electronics includes current feedback followed by a proportional gain $K_{ip}$ and an integral gain $K_{ii}$. Saturation effects are introduced to limit the allowed velocity and torque values, and the resultant torque demand signal is normalized to provide the correct $\alpha$ value. In this work, it is assumed that the described models for the power drive electronics and control scheme are appropriate for an early stage EMA model. Further developments shall explore more complicated representations for these components and its integration with the electric motor.

Regarding the electric motor modeling, a typical DC motor representation including windings dissipation $R_{motor}$ and inductance $L_{motor}$ is considered. Conversion from the electric domain to the mechanical domain is performed by a perfect gyrator element with ratio given by the torque constant $K_T$. On the mechanical domain, the rotor inertia $I_{motor}$ and a viscous friction resistance $R_{f,motor}$ are considered.

In the presented bond graph, $\Theta$ is used to represent the temperature of operation, which modulates some of the electric resistances and friction losses. Further details on the constitutive equations for the listed elements and temperature modulation are described by Fu *et al.* (2018).

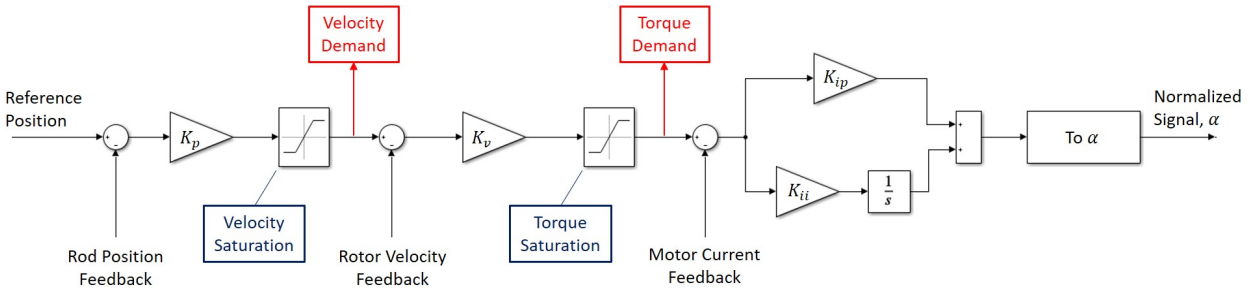


Figure 5: Schematics of the EMA controller.

### 4.2 Gear train and brakes

Modeling of the gear train is performed by considering both gears inertias ($I_{pinion}$ and $I_{gear}$) and radii ($R_{pinion}$ and $R_{gear}$). The rotary domain dynamics of the gears is converted to a translational domain by using perfect transformers associated to each radius value. Then, gear teeth contact is introduced by taking its stiffness $k_{gear}$ and structural damping $b_{gear}$ into account. The implemented compliance model is the same as the one described by Fu *et al.* (2018), which is a non-linear model capable of accounting for backlash or pre-load effects.

The dissipative element $R_{brake}$ models the effects of a braking torque, which represents the required anti-back drive effect. In this case, it is assumed a Karnopp friction model as described by Pennestri *et al.* (2016). Such model makes use of a dead-zone concept to allow the representation of stiction. The variable which modultes $R_{brake}$ is a measure of the external torque acting on the shaft, in an opposite direction to the brake torque, and is used to define if breakthrough from the stiction dead-zone occurs.

### 4.3 Screw mechanism, no-back and control surface

The screw mechanism is modeled considering its inertia $I_{nut}$ and mass $M_{screw}$. Conversion from the shaft rotation to screw linear movement is performed by using the perfect transformer and the screw lead $l_{screw}$. Similarly to the case of the gear train, the contact between nut and screw is included by using the compliance model in conjunction with the contact stiffness $k_{screw}$ and damping $b_{screw}$. Friction losses on the screw are considered by using the R-element $R_f$, which accounts for Coulomb, Stribeck and seal friction losses. Also, the friction term is affected by the temperature of operation. Friction modeling and temperature modulation are detailed and described by Fu *et al.* (2018).

Anti-back driving by means of a no-back device is already considered in the model by introducing the element $R_{no-back}$. Once again, the Karnopp friction model is used to address the stiction phenomenon, similar to the implementation of brake modeling.

Finally, the control surface installation is included by considering its inertia $I_{surf}$, structural stiffness $k_{surf}$ and damping $b_{surf}$. In this case however, linear models for the C and R elements are used. The perfect transformer which converts the screw movement to surface rotation is defined by the effective arm $b_{eff}$ from the RLC configuration as depicted in Fig. 2. As the geometry is such that $b_{eff}$ depends on the current surface position, the transformer is a modulated element. $H_{aero}$ is the aerodynamic hinge moment acting over the control surface, which is usually defined since the requirements specification stage.

### 4.4 Model realization

The bond graph representation and the description of each of its elements allow one to define the system equations. This is done by associating each C or I-element with integral causality to a state variable. Then, conservation laws for the 0 and 1-junctions are used to derive the equations. With the system equations derived and implemented in the *Simulink* environment, it is possible to run the desired simulations to observe the EMA behavior.

Analysis of the efforts acting on each one of the different components allows the observation of compliance to the load rating constraints. More important, by analysing the dynamic response for the control surface displacement and velocity, compliance to the performance requirements can be evaluated. Additionally, the temperature of operation can be varied to allow the exploration of its effects, specially when considering low-temperature conditions, in which the EMA may face performance issues due to poor lubricant behavior. Low supply voltage conditions can also be recreated to allow the study of supply network failure conditions.

## 5. CASE STUDY

This section's purpose is to demonstrate how both the EMA sizing tool and the EMA model can be used to provide valuable information in a preliminary design context. In order to do so, an example application is proposed and the sizing

tool is used to evaluate viable solutions for the required actuator. Then, the results from the sizing tool are used as inputs for the EMA model, which is used to run simulations to assess its behavior and conclude the example case.

The example case data is extracted from Ballesteros (2015), where requirements for the sizing of a rudder actuator are presented. In the example described, the actuator must deflect the surface from 0 to 30 degrees when facing an aerodynamic hinge moment of 3050 Nm. In terms of the dynamic response, it must have a maximum settling time (2% criteria) of 850 ms, with an overshoot and steady-state error lower than 10 % and 1%, respectively. Besides that, the maximum surface deflection rate must not be higher than $40°/s$, and its average value over the travel time between 15 % and 85 % of the steady-state value must be higher than $32°/s$.

### 5.1 Sizing step

As previously mentioned, the EMA sizing tool is capable of finding adequate solutions with different types of gear trains. In order to demonstrate the tool's capabilities, it is first assumed that a spur gear actuator is being evaluated. Also, it is assumed that a design with the lower overall weight is desired. Therefore, $\alpha_2$ is set to 0 in Eq. 1 at first. These informations, in combination with the listed performance requirements, are provided to the sizing module and its result is described in Tab. 1. Note that the sized actuator as described in Tab. 1 consists on the solution from the sizing tool after being adjusted to contain only off-the-shelf components from the cited catalogs. Each component is described by its respective catalog model and mass. In terms of the design variables vector $x$ used in the optimization problem, the described solution is the case where its parameters correspond to $D_{screw}$ = 15 mm, $l_{screw}$ = 10 mm, $mod_{gear}$ = 2, $N_p$ = 18, $N_g$ = 45, $T_{CS}$ = 6.1 Nm and $i_{CS}$ = 3.7 A.

Table 1: EMA configuration found from using the actuator sizing tool with the gear train type set as spur gear.

| **Component** | Ball screw | Spur gear | Electric motor | Brakes | EMA |
|---|---|---|---|---|---|
| **Model** | BLW 1510-5.6 | MSGA2-18/45 | PMA43N | TMB 2.5 | - |
| **Mass [kg]** | 1.63 | 1.24 | 7.6 | 1.2 | 11.67 |

As previously mentioned, the sizing tool can also be used to compare the effects of using different components. An example is to allow the comparison of using different types of gear trains. By setting the gear train type to helical or bevel in the sizing routine, solutions with an overall weight of 11.76 kg and 11.83 kg, respectively, are found. In this case, as the prioritized objective is to minimize the overall weight of the solution, it is shown that the spur gear selection provides a better match to the design needs. By expanding the sizing tool database with data regarding different components, it is possible to carry out similar studies comparing the use of no-back instead of brakes, or even verifying if the assumptions regarding the screw mechanism and electric motor selection are correct.

The data presented in Tab. 1 and the estimates for different gear train types indicate that an EMA with an overall mass close to 12 kg should be capable of providing the desired performance requirements (note that the sizing tool considers only the weights of the listed components, not including contributions from housing, seals, bearings, etc.). This information by itself can be used to compare the preliminary EMA with a preliminary conventional hydraulic actuator sized for the same application.

Moreover, power demand characteristics can be extracted to allow a more detailed comparison. However, as the EMA model considers a more complex actuator dynamic behavior, including switching losses, conduction dissipation, structural damping, etc., it is interesting to leave this analysis for the simulation step.

### 5.2 Simulation step

In order to validate the sized actuator from the previous step, the EMA dynamic model is used to run more detailed simulations. As the models of each one of the actuator components are now known, it is not necessary to make use of data sheet interpolations. Instead, the parameters for each model listed in Tab. 1 are extracted from the catalogs and inserted as required parameters for the simulation.

The sized actuator's capacity to comply to the required performance requirements described above is then verified. In this case, the influence of temperature on the actuator's response is not considered, as the requirements do not specify a particular condition. Also, both the reference step input with amplitude of 30° and the aerodynamic hinge moment step with amplitude of 3050 Nm (a step load is assumed as a conservative approach) are set to initiate at t = 0 s. The dynamic response obtained from the simulation over a timespan of 1.5 seconds is shown in Fig. 6.

Figure 6a shows the control surface deflection while Fig. 6b shows its deflection rate. As it can be seen from Fig. 6a, the reference input of 30° is tracked with an appropriate steady-state error and no overshoot. Moreover, the maximum deflection rate of $40°/s$ is respected. The detailed values of each one of the parameters listed as performance requirements, including the settling time and the average deflection rate, are shown in Tab. 2.

As important as the verification of the compliance to the performance requirements, is the compliance to the sizing

constraints. By analysing the efforts acting on each one of the components, the loads can be evaluated and compared with its respective load ratings. Such analysis is illustrated by the curves from Fig. 7, in which Fig. 7a shows the torque and the corresponding current on the electric motor, and Fig. 7b shows the force on the ball screw over time. In this case, the motor provides a peak torque of 21.3 Nm and the ball screw withstands a peak force of 20.7 kN. As the chosen components are capable of enduring loads up to 21.7 Nm and 27.8 N, respectively, it is shown that they are appropriate for the application. The same analysis applies for the verification of the gear train and brakes load constraints, though, for the brakes, the static torque is the sizing parameters rather than the dynamic torque response. Besides that, the motor velocity constraint can also be verified by plotting the resultant motor rotation curve.

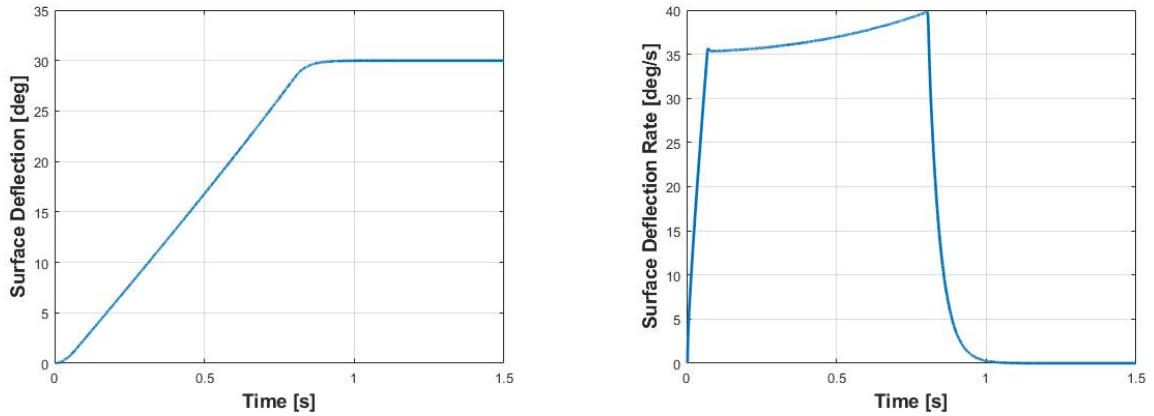


(a) Surface deflection (b) Surface rate

Figure 6: Dynamic response of the EMA sized by using the actuator sizing tool.

Table 2: Verification of performance requirements.

| **Parameter** | Steady state error | Overshoot | Settling time | Maximum rate | Average rate |
|---|---|---|---|---|---|
| **Required** | $< 1\%$ | $< 10\%$ | $< 850ms$ | $< 40°/s$ | $< 32°/s$ |
| **Obtained** | $0.02\%$ | NA | $842ms$ | $39.8°/s$ | $36.8°/s$ |

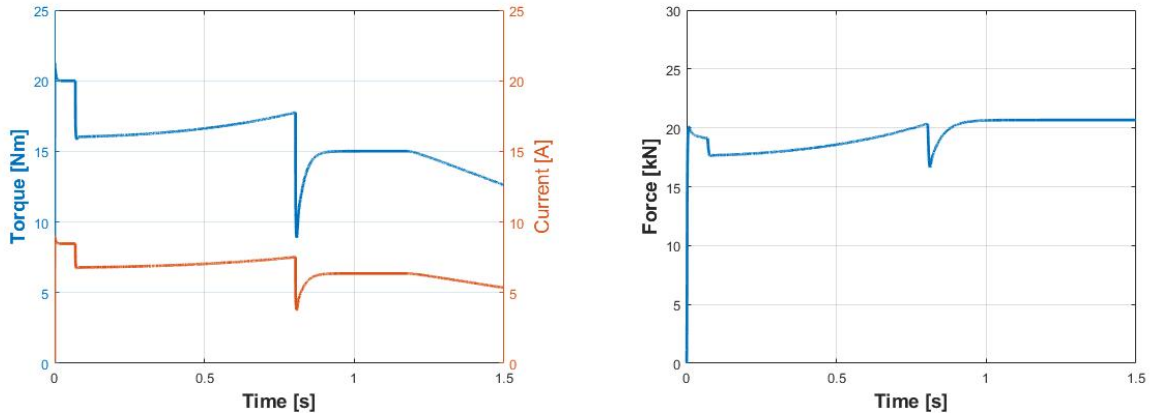


(a) Electric motor torque and current (b) Ball screw load

Figure 7: Evaluation of loads acting on the EMA components.

Finally, it is possible to evaluate the EMA power demand characteristics with a higher fidelity than it would be possible from the sizing tool calculations. The demanded power is observed at the source of effort element attached to the power drive electronics in Fig. 4. Figure 8 illustrates the power demand over time and indicates a peak demand of 3.66 kW. Also, besides not being illustrated, such demand profile results in a peak current of 9.0 A on the power drive electronics, which corresponds to the current in Fig. 7a after accounting for the PWM transformation and losses. By combining this information with the overall EMA mass estimate, it is possible to conclude the comparison with the conventional actuation technology in terms of power density. Moreover, with the expected current on the power drive electronics, it is possible to

estimate the wiring characteristics of the electric power supply network and compare it with the hydraulic supply line that would be required to power the conventional solution. Besides that, the same actuator can be evaluated when operating under different conditions (e.g.: low temperature) to allow an anticipated evaluation of the EMA capabilities in such environments.

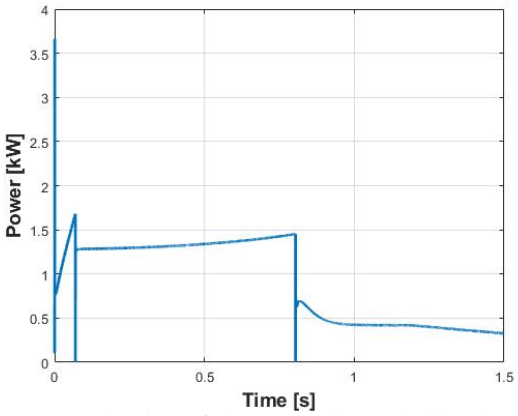


Figure 8: Evaluation of the power demanded by the EMA.

## 6. CONCLUSIONS

This work proposed the development of tools that can aid the task of evaluating the possibility of using EMAs for actuation of flight control surfaces in a preliminary design context. The use of such tools was exemplified through a case study, in which it was shown that the objective of using the sizing tool to find an optimal actuator was achieved and the compliance to the project requirements were validated from the simulations results. Also, possible analysis using the results from both tools were indicated, highlighting the utilities of using the developed routines.

Further developments shall expand the sizing tool capabilities, allowing the addition of even more components to its database (e.g.: more complex gear drives, roller screws, etc.) and the accountability of minor components contributions (housing, bearings, etc.). Also, though already included in the EMA model, no-back estimation must also be included in the sizing tool database. Another major development would include a better representation of the power drive dynamics instead of the lumped-parameters approach used in this work. This improvement shall include a behavorial model of the switching PWM and considerations on the behavior of the sensors used to provide the required control feedback.

## 7. REFERENCES

Ballesteros, H.M.S., 2015. *Dynamic Stiffness Enhancement of a Flight Control Actuator using Control Techniques*. Master's thesis, Instituto Tecnológico de Aeronáutica, São Jospé dos Campos, Brasil.

Budinger, M., Reysset, A., El Halabi, T., Vasiliu, C. and Mare, J.C., 2013. "Optimal preliminary design of electromechanical actuators". *Proceedings of the Institution of Mechanical Engineers Part G Journal of Aerospace Engineering*.

Cao, W., Mecrow, B., Atkinson, G., Bennett, J. and Atkinson, D., 2012. "Overview of Electric Motor Technologies Used for More Electric Aircraft (MEA)". *Industrial Electronics, IEEE Transactions on*, Vol. 59, pp. 1 – 1.

Fu, J., Mare, J.C., Yu, L. and Fu, Y., 2018. "Multi-level virtual prototyping of electromechanical actuation system for more electric aircraft". *Chinese Journal of Aeronautics*, Vol. 31, No. 5, pp. 892 – 913.

KHK, 2015. "KHK All Product Guide & Technical Data". https://khkgears.net/new/gear_catalog.html. Accessed 28 october 2020.

OGURA, 2012. "Electromagnetic Brake TMB Series". http://www.kpbgroup.com. Accessed 01 march 2021.

PACIFIC SCIENTIFIC, 2001. "High performance servo motors". https://www.kollmorgen.com/en-us/service-and-support/technical/pacific-scientific-pacsci-motors/. Accessed 28 october 2020.

Pennestri, E., Rossi, V., Salvini, P. and Valentini, P.P., 2016. "Review and comparison of dry friction force models". *Nonlinear Dynamics*, Vol. 83.

THK, 2020. "Ball Screw General Catalog". https://www.thk.com/catalog/?lang=en. Accessed 27 october 2020.

Todeschi, M., 2011. "Airbus - EMAs for Flight Controls Actuation System - An Important Step Achieved in 2011". In *Aerospace Technology Conference and Exposition*. SAE International.

## 8. RESPONSIBILITY NOTICE

The authors are solely responsible for the printed material included in this paper.